taken to be zero and $\frac{3}{4}\exp(B_2^{II}/kT)$ is ignored, then Eq. (51) becomes Eq. (23) which is the equation for the nearest-neighbor interaction.

## VII. CONCLUSIONS AND SUMMARY

Divacancies and trivacancies in body-centered cubic metals have been classified and discussed. For the nearest-neighbor interaction, one type of divacancy and three types of trivacancies are classified. These are 71° trivacancies, 109° trivacancies, and 180°(I) trivacancies. Divacancies have to be broken up into two single vacancies to migrate. For the next-nearest-neighbor interaction there are two kinds of divacancies. Type I has the vacant sites in the nearest-neighbor position and type II has the vacant sites in the next-nearest-neighbor position. There are three more kinds of trivacancies for the next-nearest-neighbor interactions. These are 90° trivacancies, 144° trivacancies, and 180°(II) trivacancies. The general kinetic equations are discussed in detail concerning these defects. The formation of divacancies during quenching and annealing is discussed in great detail. There exists a critical temperature $T^*$ above which the temperature is high enough to maintain thermal equilibrium but below which the motion of single vacancies is too slow to maintain thermal equilibrium in the quenching process. The situation at $T^*$ is frozen in by quenching. After the quench more divacancies are formed and the kinetic equations and the characteristic times for the formation of divacancies are discussed.

## ACKNOWLEDGMENTS

The author is grateful for the continuous interest and encouragement of J. S. Koehler and O. C. Simpson. The author is deeply indebted to J. S. Koehler and R. M. J. Cotterill for stimulating discussions. The editorial assistance of D. Larson, R. Flink, and C. Lode is deeply appreciated.

PHYSICAL REVIEW VOLUME 160, NUMBER 3 15 AUGUST 1967

# Determination of Anisotropic Momentum Distributions in Positron Annihilation

P. E. MIJNARENDS
*Reactor Centrum Nederland, Petten, The Netherlands*
(Received 1 March 1967)

A theoretical method is presented which permits the experimental determination of the momentum distribution of the photon pairs originating in positron annihilation in crystalline solids, as a function of both the magnitude and the direction of that momentum. The distribution is expanded in a series of lattice harmonics. It is shown how linear combinations of the two-quantum angular correlations, obtained from measurements on a number of suitably oriented single crystals, may be unfolded to yield the momentum-dependent coefficients in that expansion. The method is illustrated by a model computation.

## 1. INTRODUCTION

IT is well known that the angular correlation of the annihilation radiation from positrons stopped in oriented single crystals[1–5] may provide information on the electronic structure of the substance under study and, in metals, on the shape of the Fermi surface. The intensity of the two-quantum angular correlation $N(p_z)$, measured with the long horizontal slit apparatus commonly used,[2] is proportional to the probability that the photon pair carries off a momentum with a component along the $z$ axis of the instrument between $p_z$ and $p_z+dp_z$. This probability is related to the probability that the pair of annihilation quanta has a total momentum $\mathbf{p}$, i.e., the photon-pair momentum distribution $\rho(\mathbf{p})$, by

$$N(p_z) \propto \int_{-\infty}^{\infty}\int_{-\infty}^{\infty} \rho(\mathbf{p})dp_x dp_y. \quad (1)$$

In general, $\rho(\mathbf{p})$ is anisotropic owing to the presence of the lattice potential,[2] while it is also influenced by many-body effects like electron-electron and electron-positron correlations.[6,7] The detailed behavior of $\rho(\mathbf{p})$ will therefore yield information concerning those effects.

The extraction of this information from the experimental data is complicated by the fact that one does not directly measure $\rho(\mathbf{p})$ but rather its integrals over slices of momentum space characterized by certain values and orientations of $p_z$, as expressed by Eq. (1). Of

[1] S. Berko, R. E. Kelley, and J. S. Plaskett, Phys. Rev. **106**, 824 (1957).
[2] S. Berko and J. S. Plaskett, Phys. Rev. **112**, 1877 (1958).
[3] A. T. Stewart, J. B. Shand, J. J. Donaghy, and J. H. Kusmiss, Phys. Rev. **128**, 118 (1962).
[4] J. J. Donaghy, A. T. Stewart, D. M. Rockmore, and J. H. Kusmiss, in: *Proceedings of the IXth International Conference on Low Temperature Physics, Columbus, Ohio*, edited by J. G. Daunt, D. O. Edwards, F. J. Milford, and M. Yaqub (Plenum Press, Inc., New York, 1965), Part B, p. 835.
[5] B. Rozenfeld, W. Swiatkowski, and J. Wesolowski, Acta Phys. Pol. **29**, 429 (1966).
[6] S. Kahana, Phys. Rev. **117**, 123 (1960); **129**, 1622 (1963).
[7] C. K. Majumdar, Phys. Rev. **140**, A227 (1965); **140**, A237 (1965).

course one may postulate a simple model and try to fit the angular correlations computed from this model to the experimental data.[4,8] However, the various effects mentioned above influence the angular correlations in a far more complicated way than $\rho(\mathbf{p})$, which makes it difficult to disentangle them and to decide in which way the model should be altered in order to obtain an improved fit.

A better solution is to determine $\rho(\mathbf{p})$ from the measured angular correlations. Expression (1), relating the correlations to $\rho(\mathbf{p})$, can be thought of as representing the effect of the instrumental response to $\rho(\mathbf{p})$. The interpretation of a set of measured angular correlations would then split up into two parts: firstly, the purely mathematical problem of solving the integral equation (1) and thereby unfolding the angular correlations to yield the momentum distribution $\rho(\mathbf{p})$, and secondly the physical problem of the interpretation of the $\rho(\mathbf{p})$ thus obtained. In this paper, a method is presented to solve the first problem, i.e., the determination of the photon-pair momentum distribution, here considered as a quantity of interest in its own right, from a set of angular correlations, measured on a single crystal, which successively is given different orientations with respect to the $z$ axis of the apparatus. A mathematically related problem, encountered in radiology and involving the determination of a function in a plane from its line integrals along a number of straight lines in that plane, has recently been solved by Cormack.[9]

In the next two sections the mathematical details of the method are given. In Sec. 2 it is shown how the three-dimensional integral equation (1) may be replaced by a set of independent one-dimensional integral equations. These equations are solved in Sec. 3 and from their solutions the momentum distribution $\rho(\mathbf{p})$ is built up. In Sec. 4 the method is tested by applying it to a simple model.

## 2. PRELIMINARY THEORY

If many-body effects are neglected, the probability $\rho(\mathbf{p})$ of two photons being emitted with momentum $\mathbf{p}$ is proportional to

$$\rho(\mathbf{p}) \propto \sum_{\substack{\text{all}\\ \text{electrons}}} \left| \int e^{-i\mathbf{p}\cdot\mathbf{r}} \phi_+(\mathbf{r}) \psi(\mathbf{r}) d^3r \right|^2, \qquad (2)$$

where $\phi_+(\mathbf{r})$ and $\psi(\mathbf{r})$ denote, respectively, the positron and electron wave functions. Owing to the presence of the periodic lattice potential, $\rho(\mathbf{p})$ will not be spherically symmetric but will remain invariant under all operations of the point group of the crystal. $\rho(\mathbf{p})$ may then be expanded in lattice harmonics $F_{l\nu}(\Omega)$ of the proper symmetry

$$\rho(\mathbf{p}) = \sum_{l,\nu} \rho_{l\nu}(p) F_{l\nu}(\Omega), \qquad (3)$$

where the $F_{l\nu}(\Omega)$ are an orthonormal set of invariant linear combinations of spherical harmonics of order $l$, and $\Omega$ gives the orientation of $\mathbf{p}$ with respect to a suitably chosen orthogonal coordinate system. The index $\nu$ is an arbitrary label to distinguish the various harmonics of the same order and symmetry type. In the case of cubic crystals, the appropriate lattice harmonics are the Kubic harmonics of $\alpha$ type, given by Von der Lage and Bethe,[10] for which $l$ takes the values 0, 4, 6, 8, 10, 12 (twice), $\cdots$. Corresponding harmonics for other crystal systems may be derived in a simple manner.

Two orthogonal coordinate systems can now be defined. The system $R_c$ with coordinates $\xi$, $\eta$, $\zeta$ is fixed to the crystal and in orthogonal crystal systems coincides with the three principal axes. In hexagonal crystals the $\zeta$ axis is oriented along the $c$ axis, while the $\xi$ and $\eta$ axes lie in the basal plane. $\Omega$ gives the orientation of $\mathbf{p}$ with respect to $R_c$. The second coordinate system $R_a$ with Cartesian coordinates $x$, $y$, $z$ is connected to the apparatus, with the $z$ axis along the direction of incidence of the positrons and the $x$ axis in the plane of rotation of the movable detector. $R_c$ may be brought into coincidence with $R_a$ by a rotation through the Euler angles $\alpha, \beta, \gamma$ (as defined by Rose[11]). The angles $\beta$ and $\alpha$ are, respectively, the polar and the azimuthal angle of the $z$ axis with respect to $R_c$. The lattice harmonics have their simplest form when expressed with respect to $R_c$. As the integration in Eq. (1) has to be carried out in $R_a$, however, it is necessary to express them in terms of spherical harmonics with the $z$ axis as polar axis. Remembering that a lattice harmonic is a linear combination of spherical harmonics

$$F_{l\nu}(\Omega) = \sum_m a_{lm\nu} Y_l^m(\Omega) \qquad (4)$$

$$= \sum_m a_{lm\nu} \sum_{m'} D_{mm'}{}^{l*}(\alpha\beta\gamma) Y_l^{m'}(\theta,\phi), \qquad (5)$$

where $D^l(\alpha\beta\gamma)$ denotes the $2l+1$-dimensional rotation matrix representing the rotation transforming $R_a$ into $R_c$, and $\theta$ and $\phi$ are, respectively, the polar and azimuthal angles of $\mathbf{p}$ in $R_a$.

Equations (3) and (5) are now inserted into Eq. (1) and after transition to the cylindrical coordinates $h$, $\phi$, $z$ the integration over $\phi$ can be carried out, yielding

$$N_{\beta,\alpha}(p_z) \propto 2\pi \sum_{l,\nu} \sum_m a_{lm\nu} D_{m0}{}^{l*}(\alpha\beta 0) \times \int_{|p_z|}^{\infty} \rho_{l\nu}(p) Y_l^0(\theta,0) p\,dp$$

for the angular correlation $N_{\beta,\alpha}(p_z)$ measured with $p_z$ along an axis in the direction $(\beta,\alpha)$ with respect to the crystalline coordinate system $R_c$. Since

$$D_{m0}{}^{l*}(\alpha\beta 0) = [4\pi/(2l+1)]^{1/2} Y_l^m(\beta,\alpha)$$

[8] J. Melngailis and S. DeBenedetti, Phys. Rev. **145**, 400 (1966).
[9] A. M. Cormack, J. Appl. Phys. **34**, 2722 (1963); **35**, 2908 (1964).
[10] F. C. Von der Lage and H. A. Bethe, Phys. Rev. **71**, 612 (1947).
[11] M. E. Rose, *Elementary Theory of Angular Momentum* (John Wiley & Sons, Inc., New York, 1957), p. 50.

and

$$Y_l^0(\theta,0)=[(2l+1)/4\pi]^{1/2}P_l(\cos\theta)$$

(cf. Ref. 11, p. 60), one finally obtains, using Eq. (4)

$$N_{\beta,\alpha}(p_z)\propto 2\pi\sum_{l,\nu}\sum_{m}a_{lm\nu}Y_l^m(\beta,\alpha)g_{l\nu}(p_z)$$

$$\propto 2\pi\sum_{l,\nu}F_{l\nu}(\beta,\alpha)g_{l\nu}(p_z)\,, \qquad (6)$$

with

$$g_{l\nu}(z)=\int_{|z|}^{\infty}\rho_{l\nu}(p)P_l(z/p)pdp\,. \qquad (7)$$

Thus the radial part $\rho_{l\nu}(p)$ of the $l$th contribution to the total momentum distribution $\rho(\mathbf{p})$ is connected with the function $g_{l\nu}(p_z)$ by the one-dimensional integral Eq. (7).

The angular correlation can be measured with the $z$ axis along a number of different directions in a single crystal, providing a number of linear relations between these angular correlations and the unknown functions $g_{l\nu}(p_z)$

$$N_i(p_z)=\sum_j F_{ij}g_j(p_z)\,. \qquad (8)$$

Here the indices $i$ and $j$ form a shorthand notation for the pairs of labels $\beta$, $\alpha$ and $l$, $\nu$. For practical reasons the number of orientations, for which the angular correlation is measured, will be small. On the other hand the expansion in Eq. (8) is infinite. To solve the system of Eq. (8), in practice one assumes that the series converges and truncates it at a certain point. If the number of terms retained is less than the number of angular correlations measured one by conventional matrix inversion techniques[12] makes a least-squares fit of the truncated series Eq. (8) to the angular correlations. If on the other hand as many terms are retained as there are angular correlations available, the method to obtain an approximate solution of Eq. (8) is known as Houston's method.[13] In both cases a new system of linear equations is obtained expressing the various $g_{l\nu}(p_z)$ in terms of the measured angular correlations. $g_{l\nu}(p_z)$ is related to $\rho_{l\nu}(p)$ by the integral Eq. (7), which will be solved in the next section.

The present method can in principle also be applied to point slit measurements,[14] giving rise to a slightly different set of one-dimensional integral equations. However, the convenient reduction of the rotation matrices to lattice harmonics does not take place and the computations become considerably more involved.

## 3. SOLUTION OF THE INTEGRAL EQUATION

As a first step an auxiliary formula will be derived, relating the Fourier transform of $g_l(z)$ (the label $\nu$ will be dropped from now on) and the Hankel transform of $p^{1/2}\rho_l(p)$:

$$(2\pi)^{-1/2}\int_{-\infty}^{\infty}e^{-ixz}g_l(z)dz=(-i)^l x^{-1/2}\times\int_0^{\infty}p^{1/2}\rho_l(p)J_{l+1/2}(px)pdp\,. \qquad (9)$$

In order to avoid mathematical difficulties it is assumed in this section that $\rho_l(p)$ falls off faster than $p^{-5/2}$ for sufficiently large $p$, and that $g_l(z)$ and its first derivative are continuous functions of $z$. The last condition, although quite severe in theory, does not present difficulties in practice, since the finite instrumental resolution will smooth eventual kinks in the angular correlations.

To prove Eq. (9) one takes the Fourier transform of both sides of Eq. (7) and changes the order of integration on the right-hand side:

$$(2\pi)^{-1/2}\int_{-\infty}^{\infty}e^{-ixz}g_l(z)dz$$

$$=(2\pi)^{-1/2}\int_{-\infty}^{\infty}e^{-ixz}dz\int_{|z|}^{\infty}\rho_l(p)P_l(z/p)pdp$$

$$=(2\pi)^{-1/2}\int_0^{\infty}p\rho_l(p)dp\int_{-p}^{p}e^{-ixz}P_l(z/p)dz\,. \qquad (10)$$

The integration with respect to $z$ can be carried out, yielding[15]

$$\int_{-p}^{p}e^{-ixz}P_l(z/p)dz=(-i)^l(2\pi/x)^{1/2}p^{1/2}J_{l+1/2}(px)\,, \qquad (11)$$

from which Eq. (9) immediately follows. By inversion of either the Fourier or the Hankel transform, Eq. (9) permits in principle the computation of one of the functions $g_l$ and $\rho_l$ if the other one is known.

From here on one may proceed in various ways to find a solution of Eq. (7). The method described in this paper consists of inversion of the Hankel transform and performance of one of the integrations in the double integral obtained for $\rho_l(p)$. An alternative solution by expansion of $\rho_l(p)$ and $g_l(p)$ in series of, respectively, Laguerre and Hermite polynomials will not be treated here since the convergence of these series is poor when $\rho_l$ and $g_l$ are not smooth functions.

The Hankel transform

$$\int_0^{\infty}f(t)J_\mu(xt)tdt$$

of a function $f(t)$ is inverted by[16]

$$f(p)=\int_0^{\infty}J_\mu(px)xdx\int_0^{\infty}f(t)J_\mu(xt)tdt\,. \qquad (12)$$

[12] C. Lanczos, *Applied Analysis* (Sir Isaac Pitman & Sons, Ltd., London, 1964), Chap. II.

[13] W. V. Houston, Rev. Mod. Phys. **20**, 161 (1948); M. Miasek, J. Math. Phys. **7**, 139 (1966).

[14] P. Colombino, B. Fiscella, and L. Trossi, Nuovo Cimento **27**, 589 (1963).

[15] A. Erdélyi, W. Magnus, F. Oberhettinger, and F. G. Tricomi, *Tables of Integral Transforms* (McGraw-Hill Book Company, Inc., New York, 1954), Vols. 1 and 2.

[16] A. Erdélyi, W. Magnus, F. Oberhettinger, and F. G. Tricomi, *Higher Transcendental Functions* (McGraw-Hill Book Company, Inc., New York, 1953), Vol. 2, p. 73,

Let $f(p)=p^{1/2}\rho_l(p)$ and $\mu=l+\frac{1}{2}$; then

$$p^{1/2}\rho_l(p)=\int_0^\infty J_{l+1/2}(px)xdx \times\int_0^\infty t^{1/2}\rho_l(t)J_{l+1/2}(xt)tdt, \quad (13)$$

which with the aid of Eq. (9) can also be written as

$$p^{1/2}\rho_l(p)=i^l(2\pi)^{-1/2}\int_0^\infty x^{1/2}J_{l+1/2}(px)xdx \times\int_{-\infty}^\infty e^{-ixz}g_l(z)dz. \quad (14)$$

Since the integral with respect to $x$ does not converge, it is necessary first to carry out two partial integrations with respect to $z$, using the fact that both $g_l(z)$ and its derivatives vanish at infinity. These partial integrations contribute a factor $x^{-2}$ to the integrand, which makes the integration with respect to $x$ converge:

$$p\rho_l(p)=-i^l(2\pi)^{-1/2}\int_0^\infty (px)^{-1/2}j_{l+1/2}(px)d(px) \times\int_{-\infty}^\infty e^{-ixz}g_l''(z)dz. \quad (15)$$

From the defining Eq. (7) and the parity of the Legendre polynomials it follows that $g_l(z)$, and therefore also its second derivative $g_l''(z)$, are even (odd) functions of $z$ if $l$ is even (odd), while the same holds true for $y^{-1/2}\times J_{l+1/2}(y)$. This makes it possible to write the Fourier transform in Eq. (15) as a cosine (sine) transform. The order of integration is then changed and the integration with respect to $x$, now involving the cosine (sine), is written as a Fourier transform, yielding

$$p\rho_l(p)=-i^l(2\pi)^{-1/2}\int_0^\infty g_l''(z)dz \times\int_{-\infty}^\infty y^{-1/2}J_{l+1/2}(y)\exp(-iyz/p)dy, \quad (16)$$

where $y=px$. Since[17]

$$\int_{-\infty}^\infty y^{-1/2}J_{l+1/2}(y)e^{-i\omega y}dy = \begin{cases}(-i)^l(2\pi)^{1/2}P_l(\omega), & \omega^2<1,\\ 0, & \omega^2>1,\end{cases} \quad (17)$$

this can also be written as

$$\rho_l(p)=-(1/p)\int_0^p g_l''(z)P_l(z/p)dz. \quad (18)$$

After two partial integrations the final solution is then obtained:

$$\rho_l(p)=-\frac{1}{p}\left[\frac{dg_l(p)}{dp}-\frac{l(l+1)}{2p}g_l(p)+\frac{1}{p^2} \times\int_0^p g_l(z)P_l''(z/p)dz\right], \quad (19)$$

where $P_l''$ denotes the second derivative of the Legendre function with respect to its argument.

For $l=0$, i.e., for the isotropic part of $\rho(\mathbf{p})$, only the first term in Eq. (19) remains

$$\rho_0(p)=-(1/p)(dg_0(p)/dp), \quad (20)$$

which is the well-known relation first given by Stewart.[18] Equation (19) is the direct generalization of this formula for the anisotropic case.

By multiplying the various $\rho_l(p)$'s by their corresponding lattice harmonics and summing them according to Eq. (3), the total momentum distribution $\rho(\mathbf{p})$ may be constructed and plotted in a contour diagram. If desired, $\int\rho(\mathbf{p})d^3p$ may be normalized to unity by dividing $\rho(\mathbf{p})$ by a factor

$$(4\pi)^{1/2}\int_0^\infty \rho_0(p)p^2dp=(4\pi)^{1/2}\int_0^\infty g_0(p)dp,$$

i.e., by $\sqrt{\pi}$ times the area under one of the angular correlations, after these areas have been equalized.

## 4. MODEL COMPUTATION

As sufficiently accurate and extensive experimental data were not available, it was decided to test the method by applying it to a simple model. Starting from an assumed momentum distribution $\rho(\mathbf{p})$, the angular correlations were computed for a number of nonequivalent crystal orientations. Next the correlations were unfolded again following the procedure developed in the preceding sections. Finally the momentum distribution was reconstructed and compared with the model distribution.

For the model computation a fictive bcc metal crystal was chosen. Application to a metal constitutes a severe test of the method as in nonmetals the momentum distribution does not show sharp breaks. The probability $\rho(\mathbf{p})$ equaled 100 arbitrary units inside a Fermi sphere of radius $p_F$ around the origin of momentum space. Furthermore, it was assumed that the presence of higher momentum components in the wave functions of the positron and the conduction electrons results in 12 spheres, also of radius $p_F$, inside which $\rho=5$, and which are centered on the nearest neighbor sites in the fcc reciprocal lattice. The lattice constant was taken as 6.518 atomic units (a.u.) and $p_F=0.598$ (a.u.)$^{-1}$, values corresponding to lithium. Recently, Calais[19] has shown

[17] Y. L. Luke, *Integrals of Bessel Functions* (McGraw-Hill Book Company, Inc., New York, 1962), p. 321.

[18] A. T. Stewart, Can. J. Phys. **35**, 168 (1957).

[19] J. L. Calais, Arkiv Fysik **28**, 539 (1965).

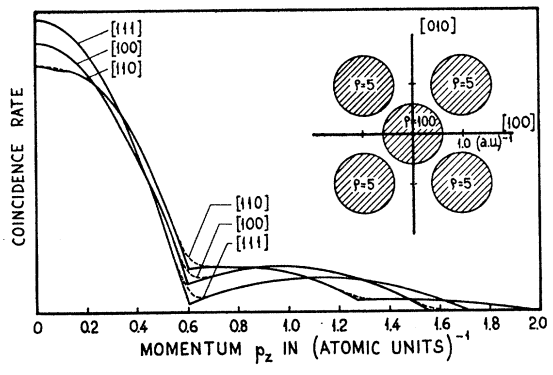


FIG. 1. Calculated angular correlations for $p_z$ along the [100], [110], and [111] directions of a fictive bcc crystal having a probability distribution as shown in the inset. Dashed curves indicate the effect of making the surface of the spheres somewhat diffuse.

how to expand such a multicentered distribution in cubic harmonics. The angular correlations, a few of which have been plotted in Fig. 1, consist of sets of inverted parabolas. A program was developed for use on an Electrologica X-8 digital computer. A variable number of crystal orientations was introduced, and the program computed either a least-squares or the Houston solution of Eq. (8). The cubic harmonics were taken from recent work of Mueller and Priestley.[20] The resulting $g_l$ functions were introduced into Eq. (19) and from the computed $\rho_l$'s the momentum distribution was reconstructed as described in Sec. 3. A separate program computed the standard deviation of each computed $\rho(\mathbf{p})$ value, which would be due to the counting statistics in an actual experiment.

The first results showed a number of sharp peaks and troughs in the reconstructed $\rho(\mathbf{p})$ distribution. This is to be expected as the parabolic angular correlations for this model show sharp kinks at the various cutoff angles, such that the differentiability condition on the $g_l$ functions is not fulfilled. This problem was circumvented by making the surface of the spheres somewhat diffuse, thus simulating a finite instrumental resolution. Mathematically, such a diffuse sphere of average radius $p_F$, centered at $\mathbf{q}$, may be described by

$$\rho(\mathbf{p}) = A_0 \operatorname{Erfc}\lambda(|\mathbf{p}-\mathbf{q}|-p_F),$$

where $\lambda$ is a constant large compared with $1/p_F$, determining the thickness of the diffuse shell, $A_0$ is the value of $\rho(\mathbf{p})$ at the center of the sphere, and

$$\operatorname{Erfc}(x) = \pi^{-1/2}\int_x^\infty \exp(-t^2)dt.$$

The angular correlations remain parabolic except for narrow regions having a width of the order of $1/\lambda$ around the cutoff points, where some rounding off takes place (dashed curves in Fig. 1). For most computations,

[20] F. M. Mueller and M. G. Priestley, Phys. Rev. 148, 638 (1966).

TABLE I. Orientations $[hkl]$ of $p_z$ for the angular correlations used in the reconstruction of $\rho(\mathbf{p})$, shown in Figs. 2 and 3.

| Figs. 2(b) and 3(b) $h$ $k$ $l$ | Figs. 2(c) and 3(c) $h$ $k$ $l$ | Figs. 2(d) and 3(d) $h$ $k$ $l$ |
|---|---|---|
| 1 0 0 | 1 0 0 | 1 0 0 |
| 1 1 0 | 1 1 0 | 1 1 0 |
| 1 1 1 | 1 1 1 | 1 1 1 |
| | 2 1 0 | 2 1 0 |
| | 1 1 2 | 1 1 2 |
| | 2 2 1 | 2 2 1 |
| | | 1 1 4 |
| | | 1 3 4 |
| | | 3 3 4 |
| | | 4 1 0 |
| | | 1 2 4 |
| | | 4 3 0 |

a value of $\lambda = 20$ a.u. was used, corresponding to a resolution of about 0.6 mrad. A large number of cases was computed in which the number of correlations, the directions of $p_z$, and the number of terms retained in Eq. (8) were varied. As soon as the number of angular correlations became larger than about four, the Houston method started to produce wildly fluctuating results for $\rho(\mathbf{p})$. This is not unexpected because it is always possible to fit a function containing $n$ disposable parameters to $n$ prescribed values, but in the intervals between the points at which the function is fitted, there are no restraints on its behavior.

The least-squares inversion of Eq. (8), on the other hand, gave useful results provided the number of terms retained was equal to about half the number of angular correlations. Figures 2 and 3 show some results for cases in which the correlations were computed with $p_z$ in directions with low Miller indices, listed in Table I. The dashed straight lines indicate the Brillouin zone boundaries. The central Fermi sphere, represented by the 50 units contour, is well reproduced in all cases. Furthermore, it is clear that the representation of details in the neighboring Brillouin zones, such as the higher momentum spheres, rapidly improves when more angular correlations are available. The distribution shown in Fig. 2b, obtained from three angular correlations with $p_z$ respectively, along the [100], [110], and [111] axes, is rather unsatisfactory. It can be improved [Fig. 2(c)] by adding three more correlations and making a least-squares fit of $g_0$, $g_4$, and $g_6$. The additional information contributed by the extra three correlations results in smaller troughs on the [100] axes and between the central and the secondary spheres, and in smaller fluctuations within the secondary spheres. On the other hand, it will also be clear from these plots that the number of correlations required to obtain a major improvement in the reproduction of the higher momentum spheres becomes impractically large. In practice, a certain amount of distortion due to termination errors will therefore be unavoidable.

The question may be asked whether crystal orientations other than the chosen ones might not give better

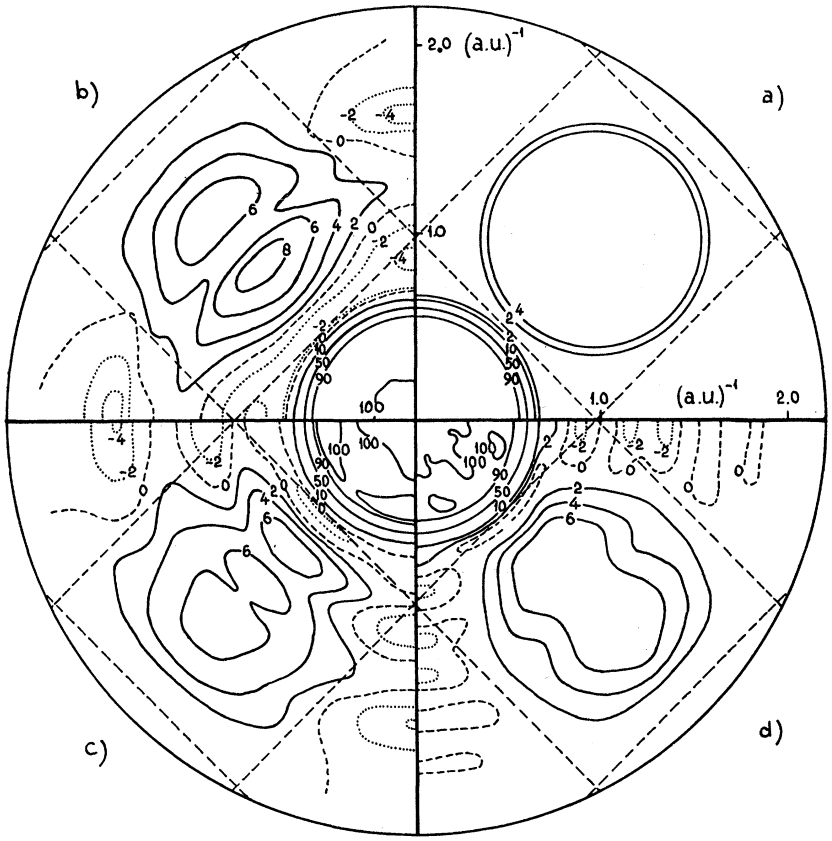


FIG. 2. Reconstructed photon-pair momentum distributions $\rho(\mathbf{p})$ in the (001) plane using various numbers of angular correlations ($AC$'s). (a) Theoretical distribution; (b) reconstructed distribution using 3 terms obtained from 3 $AC$'s (Houston's method); (c) same, using 3 terms obtained from a least-squares fit to 6 $AC$'s; (d) same, using 6 terms from a least-squares fit to 12 $AC$'s. The orientations of $p_z$, for which the $AC$'s have been determined, are listed in Table I.

results. In order to get an impression of this, a few cases were computed with a set of crystal orientations given in Table II and described by Miller indices $hkl$ with $l=1$ and $h$ and $k$ arbitrary (but not simple) fractions. Figure 4 shows the result of two of these computations, in which three and six correlations, respectively, were used to determine the first three terms of the series Eq. (3). Comparison with Figs. 2 (b) and (c) shows that especially the three-correlation case yields far better results than the corresponding one starting from correlations with $p_z$ in directions of high symmetry. The explanation of this fact can be found in the expression [Eq. (18)] for the $\rho_l$ functions. The integrand has pronounced maxima at the points of maximum curvature of the angular correlations, i.e., in the narrow intervals around the cutoff points of the inverted parabolas. If $p_z$ is chosen along an axis of high symmetry, the projections on that axis of a large number of secondary spheres coincide. As a result the integrand of Eq. (18) will show a small number of very pronounced maxima, and the $\rho_l$ function will exhibit a few slow oscillations of a large amplitude around its proper value. If, on the other hand, the angular correlations are computed for $p_z$ lying in directions of low symmetry as in Fig. 4, the projections of the secondary spheres on these directions will not coincide. The $\rho_l$ functions will then rapidly fluctuate with a small amplitude around their proper values, and the resulting $\rho(\mathbf{p})$ distribution will be a closer approximation of the theoretical one. Thus it is found that the common practice of measuring only a few angular correlations for $p_z$ oriented along the axes of highest symmetry is unfavorable for the accurate determination of the $\rho(\mathbf{p})$ distribution.

It was furthermore noted that peaks in the model distribution were well reproduced only when not too sharp. A few computations were made in which the secondary spheres were replaced by Gaussian peaks centered at the nearest neighbor sites. The width of these Gaussians could be varied. Broad peaks presented no problems, but when their width was gradually decreased a broadening occurred, first of all in the tangential directions. Only for very sharp peaks some broadening in radial direction was noticeable, but long before that many

TABLE II. Orientations $[hkl]$ of $p_z$ for the angular correlations used in the reconstruction of $\rho(\mathbf{p})$, shown in Fig. 4.

| Fig. 4(a) | | | Fig. 4(b) | | |
|---|---|---|---|---|---|
| $h$ | $k$ | $l$ | $h$ | $k$ | $l$ |
| 0.15 | 0.09 | 1.00 | 0.15 | 0.09 | 1.00 |
| 0.65 | 0.85 | 1.00 | 0.65 | 0.85 | 1.00 |
| 0.16 | 0.79 | 1.00 | 0.16 | 0.79 | 1.00 |
| | | | 0.14 | 0.44 | 1.00 |
| | | | 0.33 | 0.81 | 1.00 |
| | | | 0.42 | 0.61 | 1.00 |

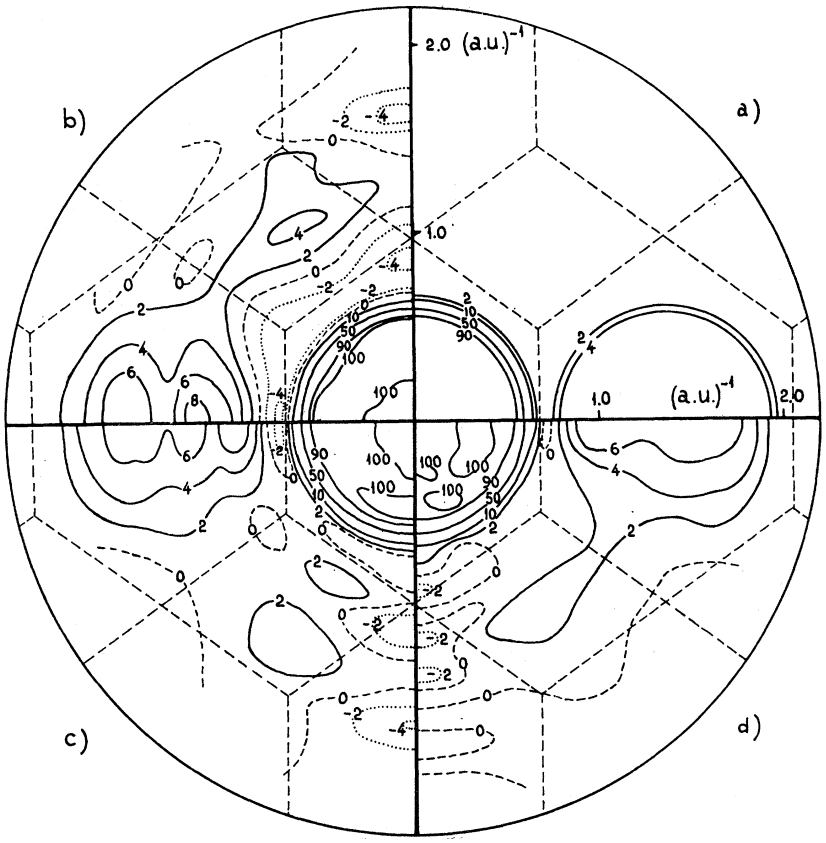


FIG. 3. Same as Fig. 2, but in the (110) plane.

parasitic peaks and troughs had started to appear at various positions, increasing in amplitude and sharpness as the Gaussians were narrowed, and rendering the result useless.

The question of how far the systematic errors described above are acceptable is closely connected to the extent to which the uncertainty due to counting statistics manifests itself in the final $\rho(\mathbf{p})$ distribution. Equation (19) has the property of strongly amplifying variations in the $g_l$ functions, especially if $l$ becomes large.

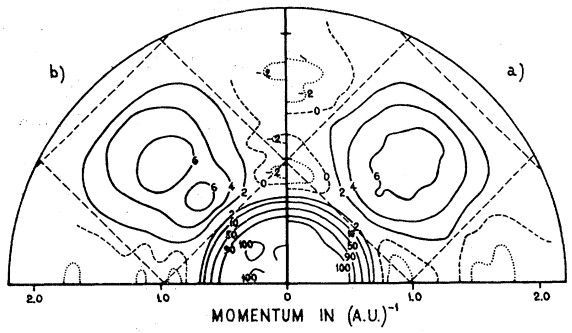


FIG. 4. Reconstructed photon-pair momentum distributions $\rho(\mathbf{p})$ in the (001) plane starting from $AC$'s with $p_z$ along directions of no particular symmetry. (a) 3 terms obtained from 3 $AC$'s; (b) 3 terms obtained from 6 $AC$'s. Table II gives the orientations of $p_z$ used to determine the $AC$'s.

Incorporation of more terms into the series Eq. (3) will therefore cause a rapid increase of the statistical uncertainty in $\rho(\mathbf{p})$, which after a certain point will offset the improved reproduction. Thus if the total duration of a measurement to determine $\rho(\mathbf{p})$ is assumed to be fixed there exists an optimum between the distortion by systematic errors and the uncertainty stemming from statistical errors.

In order to gain some insight into the latter source of error, the standard deviation $\sigma(\mathbf{p})$ of each value $\rho(\mathbf{p})$, caused by the statistical uncertainty in the angular correlations, was computed separately and plotted in the same way as $\rho(\mathbf{p})$. A striking feature is its pronounced anisotropy, with strong maxima in the [100], [110], and [111] directions. In many cases $\sigma$ was found to vary with angle by a factor of 2 or more. The choice of the crystal orientations, for which the angular correlations are determined, is also of importance. The arbitrarily chosen orientations used in Fig. 4 yield a standard deviation $\sigma(\mathbf{p})$, which consistently lies 10 to 40% higher than the corresponding quantity for the distribution of Figs. 2 (b) and (c), obtained from crystal orientations of high symmetry. The reason for this increased sensitivity to the statistics of the angular correlations is not immediately apparent, nor has it become clear whether the directions of high symmetry are the most favorable ones from the point of view of statistics.

Quantitatively, all these results are, of course, strictly valid for the chosen model only. It is felt, however, that in a qualitative sense the observations described in this section will have a more general validity, irrespective of the model. The model chosen here is a rather severe test of the method, as real metals, especially those of cubic symmetry, are often considerably less anisotropic, so a better reproduction of the actual probability distribution may be expected. The next step therefore ought to be a real, high-accuracy experiment on a metal with a well-known Fermi surface in order to see how well the shape of the Fermi surface can be derived from positron annihilation measurements. Such an experiment is presently being set up at this institute.

## 5. SUMMARY

In the present paper, a method has been developed to reconstruct the two-quantum momentum distribution from a number of angular correlations, measured for various orientations of a single crystal. In order to obtain a reliable picture of the momentum distribution, a considerably larger than usual number of correlations may be required. Moreover, if only a few correlations are measured, the common practice of choosing $p_z$ along axes of highest symmetry is unfavorable for an accurate determination of the momentum distribution. Distributions with a smoothly varying angular dependence are expected to be reproduced rather well, but difficulties may be experienced with distributions showing sharp peaks in certain directions. If the total measuring time is kept fixed, there exists an optimum between the effects of systematic and statistical errors. The position of this optimum depends on the choice of the set of crystal orientations for which the angular correlations are determined.

## ACKNOWLEDGMENTS

The author gratefully acknowledges the continuous interest and constructive criticism offered to him by Dr. B. O. Loopstra during the course of this work. He is also greatly indebted to Professor A. T. Stewart for his suggestion of the model and for interesting discussions. Thanks are further due to F. D. Dekker for several discussions and to D. van Ligten for programming assistance.

---

PHYSICAL REVIEW VOLUME 160, NUMBER 3 15 AUGUST 1967

# Quantitative Determination of Sources of the Electro-Optic Effect in $LiNbO_3$ and $LiTaO_3$

I. P. KAMINOW AND W. D. JOHNSTON, JR.
*Bell Telephone Laboratories, Crawford Hill Laboratory, Holmdel, New Jersey*
(Received 27 March 1967)

The electro-optic effect in crystals can be separated into two types of microscopic interaction: an electron-lattice contribution in which the applied field produces a lattice displacement, which in turn modifies the electronic polarizability (or refractive index), and a direct electron-field contribution in which the applied field modifies the electronic polarizability in the absence of lattice displacements. The latter contribution in $LiNbO_3$ and $LiTaO_3$ can be estimated from second-harmonic-generation experiments by Miller and Savage, and accounts for less than 10% of the refractive-index change. Each polar-lattice optic mode in $LiNbO_3$ and $LiTaO_3$ ($4A_1+9E$) contributes separately to the electro-optic effect an amount proportional to the product of its Raman-scattering efficiency and infrared oscillator strength. We have measured the absolute scattering efficiencies for $LiNbO_3$ and $LiTaO_3$. The oscillator strengths for $LiNbO_3$ have been measured by Barker and Loudon. We find that the dominant contribution to the electro-optic coefficients $r_{33}$ and $r_{13}$ comes from the lowest-frequency $A_1$ mode; and to $r_{42}$ and $r_{22}$ from the next lowest $E$ mode. These same modes dominate the low-frequency dielectric constant. The absolute values of $r_{13}$, $r_{33}$, $r_{42}$, and $r_{22}$ calculated from the combined Raman, infrared, and second-harmonic-generation data are in excellent agreement with the electro-optic coefficients measured directly by Turner. In addition to the absolute scattering efficiencies for all the transverse and longitudinal modes in $LiTaO_3$ and $LiNbO_3$, we have also determined the mode frequencies and linewidths, which are important in calculating Raman gain.

SPONTANEOUS Raman scattering is a form of light modulation that is produced by thermally excited lattice modes. In a piezoelectric crystal, some of these same modes can be excited by an externally applied electric field to produce light modulation by means of the linear electro-optic effect. We derive[1] a simple relationship between an electro-optic coefficient measured at

[1] I. P. Kaminow, in *Ferroelectricity: Proceedings of the Symposium on Ferroelectricity, General Motors Research Laboratories, Warren, Michigan, 1966* (Elsevier Publishing Company, Inc., Houston, Texas, to be published).